ISSN 2070-2051, Protection of Metals and Physical Chemistry of Surfaces, 2016, Vol. 52, No. 4, pp. 714–720. © Pleiades Publishing, Ltd., 2016.

PHYSICOCHEMICAL PROBLEMS OF MATERIALS PROTECTION

# Study of Inhibition Effect of Pyridinium Salt Derivative on Corrosion of C1010 Carbon Steel in Saline Solution[1]

**Mehdi Salih Shihab[a], *, Mehdi Honarvar Nazari[b], and Laura Fay[c]**

[a] *Al-Nahrain University, College of Science, Department of Chemistry, Al-Jadrya, Baghdad, Iraq*

[b] *Department of Civil and Environmental Engineering, Washington State University, PO Box 642910, Pullman, WA 99164-2910, USA*

[c] *Western Transportation Institute, Montana State University, P O Box 174250, Bozeman, MT 59717, USA*

*e-mail: mehdi_shihab@yahoo.com*

Received May 11, 2015

**Abstract**—In this work, pyridinium dibromide (**2**) was synthesized and its structure was confirmed using spectroscopic techniques. Compound (**2**) was successfully applied as a corrosion inhibitor for C1010 carbon steel in 3.5% NaCl solution at 25°C. Different electrochemical measurements such as potentiodynamic polarization (PDP), and electrochemical impedance spectroscopy (EIS) were used to evaluate different concentrations of the suggested inhibitor (**2**). The results showed that inhibition efficiencies obtained from EIS curves are in consistence with the results of PDP at higher concentration $4.5 \times 10^{-4}$ M. Semi-empirical calculations with PM3 method was used to find relationship between molecular structure and inhibiting effect of suggested inhibitor (2).

**DOI:** 10.1134/S2070205116040213

## 1. INTRODCTION

When steel is exposed to an aerated neutral and dilute solution of sodium chloride in water, the corrosive attack will begin at defects on the surface of steel; such as oxide films. This attack can cause destruction or degradation of metal. Due to these harmful effects, many methods have been developed to reduce or prevent the corrosion. Organic inhibitors are used for the control of corrosion of metals and alloys by creating a thin film that prevents access of corrosive agents to the metal surface. Almost all of the organic molecules which contain heteroatoms such as nitrogen, sulphur, phosphorous, and oxygen show significant inhibition efficiency [1, 2]. Inhibitors can be applied in a variety of industrial applications such as cooling systems, refinery units, pipelines, chemicals, oil and gas production units, boilers and water processing, paints, pigments, lubricants, etc. [3].

Schiff base compounds as corrosion inhibitors in acidic media were used for various metals and alloys such as mild steel, aluminum and copper [4–8]. Schiff base ligands are capable of forming stable complexes with metal ions [9]. Therefore, these compounds have wide applications and large potential in corrosion and protection area. Chito-oligosaccharide Schiff base derivatives were investigated as corrosion inhibitors for mild steel in 3.5% NaCl solution at different concentrations [10].

Quaternary ammonium bromides of different heterocyclic compounds were investigated as corrosion inhibitors of mild steel in 1 M HCl using gravimetric and polarization techniques. The inhibitor efficiency was found to be depend on the both concentration and molecular structure of the inhibitor [11]. Cetylpyridinium chloride showed high inhibition efficiency for the corrosion of low carbon steel in 1 M $H_2SO_4$ with protection efficiencies up to 97% [12]. El Achouri et.al, have also synthesized 1,2-ethanediyl bis-(dimethylalkylammonium bromide) and studied their inhibitive effect on the corrosion of iron in hydrochloric acid solution [13].

In the present work, we studied the inhibition corrosion properties of different concentration of pyridinium bromide derivative (2) for the of C1010 carbon steel in 3.5% NaCl solution. Potentiodynamic polarization (PDP) and electrochemical impedance spectroscopy (EIS) were used for investigating the corrosion behavior.

## 2. EXPERIMENTAL

### *2.1. Materials and Synthesis*

All chemical materials were used as received without further purification. Pyridinium bromide derivative inhibitor, namely: 4,4'-(2,2'-(1,4-phenylene)

[1] The article is published in the original.

bis(methanylylidene) bis (hydrazinecarbonyl)) bis(1-benzylpyridin-1-ium) dibromide (2) was synthesized by two steps, as follows:

—Preparation of *N*',*N*''-[benzene-1,4-diyldimethylylidene] dipyridine-4-carbohydrazide (1): A mixture of terephthalaldehyde (0.01 mol), abs. methanol (20 mL) and isonicotinylhydrazine (0.01 mol) with a few drops of glacial acetic acid was refluxed for 8 h. After cooling to room temperature, the precipitate was filtered and dried. The product was crystallized from ethanol [14]. Yield 65%, m.p. = 355°C (dec.). FTIR (ZnSe) $cm^{-1}$, 3240 (N–H, amide), 1652 (C=O), 1531 (C=N).

—Preparation of compound (**2**): A mixture of benzyl bromide (0.02 mol), DMSO (20 mL) and compound (**1**) (0.01 mol) refluxed for 24 h. After cooling to room temperature, the mixture was added into 30 mL of methanol. The precipitate was filtered. The product was washed with methanol two times and dried [15]. Yield 72%, m.p. = 285–287°C. FTIR (ZnSe) $cm^{-1}$, 3242 (N-H, amide), 2891 ($CH_2$ aliphatic), 1652 (C=O), 1532 (C=N). $^1$HNMR (600 MHz, DMSO-$d_6$) δppm: 5.90 (m, 2H, $CH_2$ aliphatic), 7.45–7.90 and 8.80 (m, H-Ar), 9.50 (s,1H, NH-amide). The chemical steps that included preparing the suggested Inhibitor (**2**) are shown in Scheme 1.

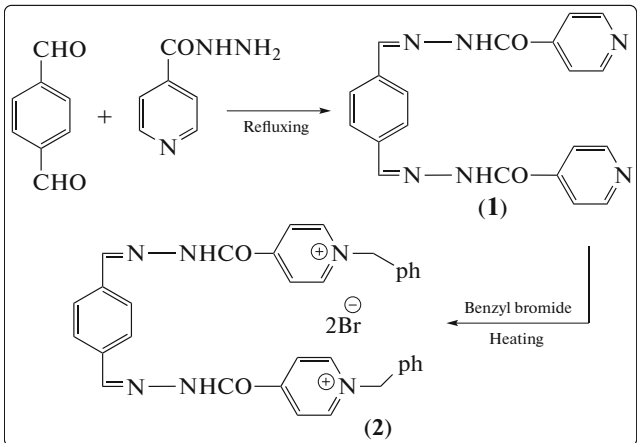


**Scheme 1.** Preparation scheme of pyridinium bromide derivative (**2**).

### *2.2. Test Material*

The experiments were carried out with C1010 carbon steel specimens. Square specimens with an exposed area of (1 $cm^2$) were encapsulated in epoxy resin as a working electrode. The surface of working electrodes were wet polished using emery papers up to 1500 grit and then cleaned with deionized water, alcohol, and finally acetone.

### *2.3. Test Solution*

The saline solutions with 3.5% NaCl were prepared by using deionized water. The concentrations range of inhibitor employed was $7 \times 10^{-6}$ to $4.5 \times 10^{-4}$ M.

### *2.4. Electrochemical Measurements*

Corrosion behavior was studied by means of electrochemical techniques such as potentiodynamic polarization (PDP), and electrochemical impedance spectroscopy (EIS). Polarization curves were recorded at a constant sweep rate of 1 mV $s^{-1}$ at the interval from –500 to +500 mV respect to the open circuit potential (OCP). The experiments were designed with a conventional three-electrode cell assembly using Potentiostat/Galvanostat/ZRA (Gamry, Reference 600). The working electrode was C1010 carbon steel. A saturated calomel electrode (SCE) was used as the reference electrode and platinum gauze was employed as the counter electrode. The linear polarization resistance was carried out at ±0.015 V with respect to the corrosion potential at a sweep rate of 0.125 mV $s^{-1}$. The polarization was carried out at cathodic potential of –0.3 V to an anodic potential of +0.3 V with respect to the corrosion potential at a sweep rate of 1 mV $s^{-1}$. The Tafel plots of anodic and cathodic curves were extrapolated to corrosion potential to get the values of corrosion current, $I_{corr}$. Electrochemical impedance measurements were carried out at open circuit potential after immersing the mild steel specimen in experimental solution in the frequency range of 10 kHz to 0.1 Hz. Applied voltage of sinusoidal wave was 10 mV. All of electrochemical measurements were carried out after the open circuit potential of the system was stabilized (after 3–4 hours immersion time). In addition, tests were conducted at room temperature (25°C).

The Gamry device was controlled by a desktop computer with DC105 DC Corrosion Software License and EIS300 Electrochemical Impedance Software License. Data analysis achieved by Gamry echem analyst version 6.24.

## 3. RESULTS AND DISCUSSION

The polarization parameters $E_{corr}$, $i_{corr}$, anodic and cathodic Tafel slopes ($\beta_a$, $\beta_c$) obtained from polarization measurements are given in the Table 1. It is clear that the values of corrosion current density decreases significantly with increasing of pyridinium salt derivative concentrations. Corrosion potential values decrease with increase in the concentration of pyridinium salt derivative. The change in the values of corrosion current density and corrosion potential in different concentrations of pyridinium salt reflected positively on the percentage inhibition efficiencies. It is evident that increasing inhibitor concentrations leads to accumulating layers of pyridinium salt caused reducing in the rate of corrosion, and then increasing

**Table 1.** Electrochemical polarization parameters for C1010 carbon steel in 3.5% NaCl solution containing different concentrations of pyridinium salt derivative at 25°C

| No. | Inhibitor concentration, M | Tafel slopes, mV/decade | | $E_{corr}$, mV | $i_{corr}$, μA/cm$^2$ | Inhibition efficiency, %[a] |
|---|---|---|---|---|---|---|
| | | $\beta_a$ | $\beta_c$ | | | |
| 1 | Uninhibited | 223.3 | 120.5 | –766 | 14.1 | – |
| 2 | $7 \times 10^{-6}$ | 170.3 | 105.9 | –735 | 10.0 | 28.5 |
| 3 | $4.5 \times 10^{-5}$ | 228.0 | 151.9 | –699 | 7.9 | 44.0 |
| 4 | $7 \times 10^{-5}$ | 366.8 | 321.0 | –646 | 7.1 | 50.0 |
| 5 | $1.5 \times 10^{-4}$ | 144.9 | 383.3 | –681 | 6.3 | 55.3 |
| 6 | $4.5 \times 10^{-4}$ | 335.3 | 155.0 | –435 | 1.0 | 91.1 |

[a] EI% = $1 - (i_{corr(inh)}/i_{corr(uninh)})$.

the percentage corrosion inhibition efficiency. However, the accumulation of molecules that adsorbed is given additional resistance to corrosion of the metal in addition to occupying reactive sites directly. We believed that higher corrosion inhibition efficiency in suggested inhibitor (**2**) is attributed to the presence of delocalized π-electrons and lone pair of electrons on nitrogen atom. Polarization curves for carbon steel in 3.5% NaCl solution at different inhibitor concentrations at 25°C are shown in Fig. 1. In addition, the $\beta_a$ and $\beta_c$ values for the inhibitor (see Table 1) were found to be changed with inhibitor concentration, which indicates that the inhibitor affected both the anodic and the cathodic reactions. Furthermore, a positive shift was observed (see Table 1) in the $E_{corr}$ values in the presence of different concentrations of inhibitor (**2**), suggesting that organic inhibitor behaves as a type of anodic inhibitor [16, 17].

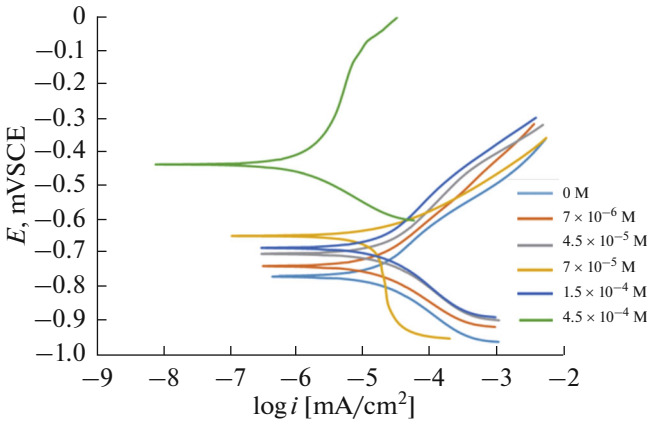


**Fig. 1.** Effect of pyridinium salt derivative concentrations in the polarization curves for C1010 carbon steel in 3.5% NaCl solution at 25°C.

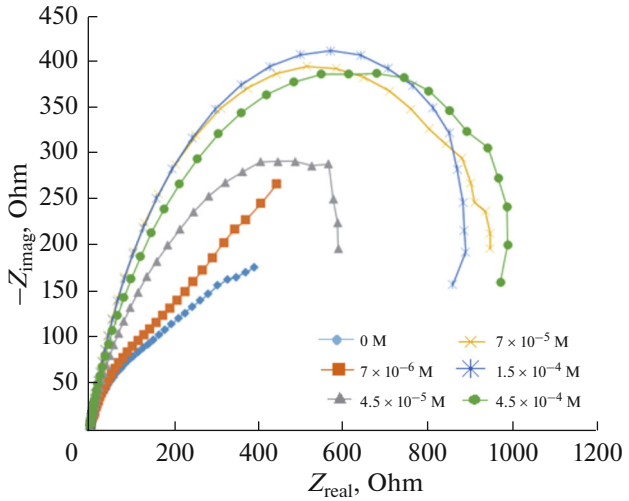


**Fig. 2.** EIS data in the Nyquist format for C1010 carbon steel in uninhibited and inhibited 3.5% NaCl solution at 25°C.

The impedance Nyquist plots of C1010 carbon steel in uninhibited and inhibited 3.5% NaCl solutions using different concentrations of pyridinium salt are shown in Fig. 2. It is clear from Fig. 2 that the protection response of carbon steel was modified in the presence of different concentrations of pyridinium salt. It can be concluded that an increase in the surface metal impedance has happened with the increase in the inhibitor concentration. Similar shape of semicircles depicted that inhibition process followed the same mechanism of corrosion inhibition. We can recognize that Nyquist plots are not completely semicircles due to frequency dispersion which could be due to roughness and in-homogeneities of the working electrode surface because of corrosion attack [18, 19]. Also Nyquist plots showed that the semicircle of the capacitive loop becomes larger in the presence of inhibitor in solution than that in the absence of inhibitor due to increase the impedance of inhibited substrate with increasing the inhibitor concentration. Adsorption of the inhibitor on the metal surface caused changing in its homogeneity, and then changing in the impedance behavior of solid metal electrodes [20, 21].

Bode modulus diagrams, Fig. 3a, show the ascending trend of low frequency impedance values is obviously seen with increasing the concentrations of pyridinium salt in 3.5% NaCl solutions. An important idea

can be taken from the Bode phase plots, Fig. 3b, is that the more concentration of inhibitor results the higher maximum phase angle, reflecting a capacitive behavior which is related to the increase of polarization resistance in the presence of inhibitor. The tendency of AC current to pass through the resistor in the circuit leads to a drop in the phase angle. Hence, the system exhibiting higher resistance can be characterized by higher phase angle.

For this case, a non-ideal frequency behavior is setup causing distributed circuit elements in the equivalent circuits. When capacitors of EIS data do not behave ideally, they act like a constant phase element (CPE). The impedance of the CPE is expressed as in Eq. (1):

$$Z_{CPE} = \frac{1}{Y_0 (i\omega)^n}. \quad (1)$$

Where $Y_0$ is the magnitude of the CPE, $-1 \leqslant n \leqslant 1$. The higher frequency range loops have depressed semicircular appearance, $0.5 \leqslant n \leqslant 1$, which is often referred to the frequency dispersion as a result of the non-homogeneity or the roughness of the solid surface [22, 23].

Figure 4 demonstrated the electrical identical circuit utilized to investigate the impedance spectra. Good fit with this model was acquired for all measurements data. The EIS corrosion measurements revealed experimental results of C1010 carbon steel in the presence and absence of inhibitor (**2**) at 25°C are summarized in Table 2. This Table listed the values of the parameters of EIS corrosion measurements ($R_s$, $R_{ct}$) by EIS fitting as well as the derived parameters $C_{dl}$ and IE%. The $C_{dl}$ values derived from CPE parameters according to Eq. (2).

$$C_{dl} = \left(Y_0 R_{ct}^{1-n}\right)^{1/n}. \quad (2)$$

Generally, the higher $R_{ct}$ values are associated with slow rate of corrosion system [24]. The decrease in the $C_{dl}$ values can be attributed to the decrease of the local dielectric constant or the increase of thickness of the electrical double layer caused by organic inhibitor molecules due to their interfering at the metal-solution interface. It's clear from Table 2 that $R_{ct}$ values

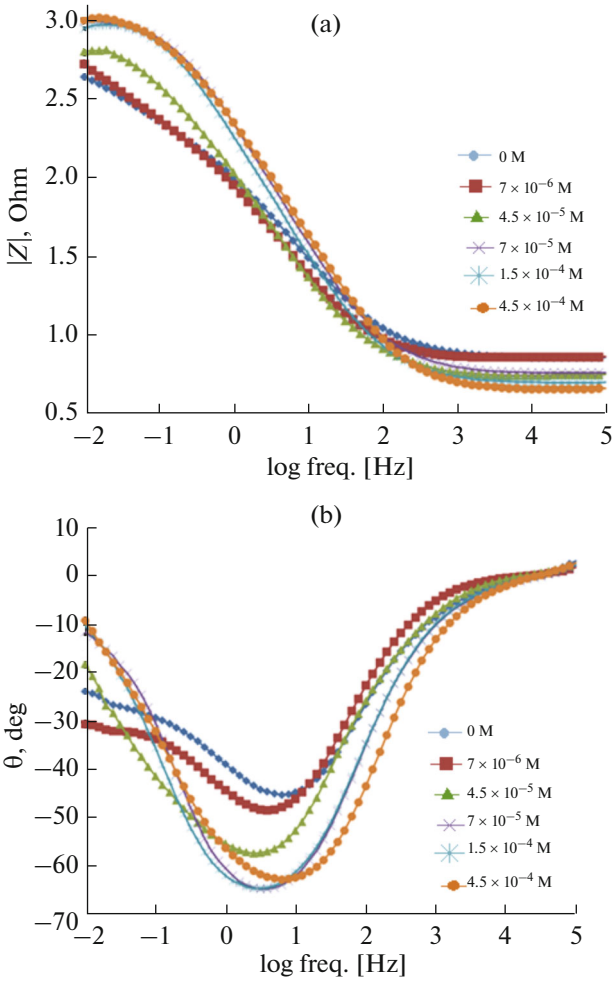


**Fig. 3.** EIS data in the Bode modulus (a) and Bode phase (b) plots for C1010 carbon steel in uninhibited and inhibited 3.5% NaCl solution at 25°C.

**Table 2.** Impedance data for C1010 carbon steel in 3.5% NaCl solution for various concentrations of pyridinium salt derivate at 25°C

| No. | Inhibitor Concentration, M | $R_{ct}$, ohm cm$^2$ | $R_s$, ohm cm$^2$ | $C_{dl}$, F cm$^{-2}$, $\times 10^3$ | $CPE_{dl}$ | | IE%[a] |
|---|---|---|---|---|---|---|---|
| | | | | | $Y_0$, S s$^\alpha$ cm$^{-2}$, $\times 10^3$ | α | |
| 1 | Uninhibited | 154.6 | 7.1 | 7.77 | 4.41 | 0.70 | – |
| 2 | $7 \times 10^{-6}$ | 189.1 | 16.5 | 3.11 | 4.08 | 0.49 | 18.2 |
| 3 | $4.5 \times 10^{-5}$ | 820.2 | 5.4 | 3.55 | 2.62 | 0.71 | 81.2 |
| 4 | $7 \times 10^{-5}$ | 1062.1 | 5.8 | 1.32 | 1.03 | 0.78 | 85.4 |
| 5 | $1.5 \times 10^{-4}$ | 1056.3 | 5.0 | 1.37 | 1.25 | 0.79 | 85.4 |
| 6 | $4.5 \times 10^{-4}$ | 1106.1 | 4.4 | 1.12 | 1.05 | 0.76 | 86.1 |

[a] IE% = $(1 - R_{ct(uninh)}/R_{ct(inh)}) \times 100$.

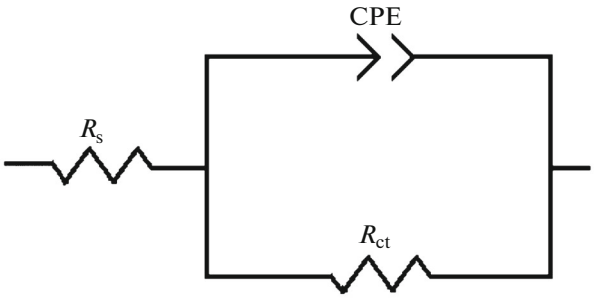


**Fig. 4.** Schematic diagram for electrochemical equivalent circuit estimated to fit the impedance measurements that contain a solution resistance ($R_s$), a constant phase element (CPE) and a polarization resistance or charge transfer ($R_{ct}$).

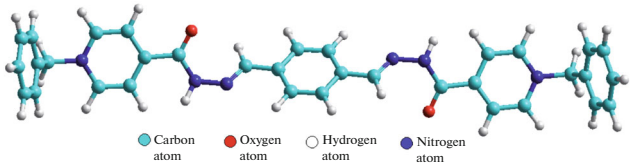


**Fig. 5.** More energetically stable conformations of pyridinium salt derivative with PM3 method.

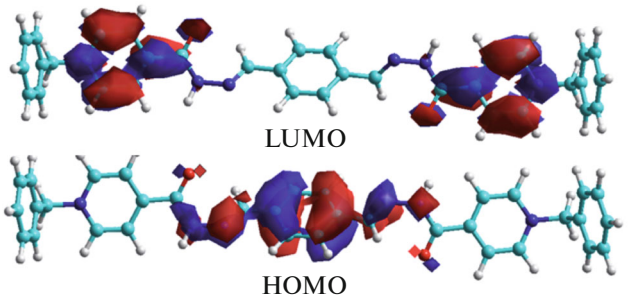


**Fig. 6.** The frontier molecular orbital density distributions (HOMO and LUMO) for pyridinium salt derivative by using PM3 method.

increase with increasing the concentration of corrosion inhibitor due to the formation of a protective film; made by corrosion inhibitor molecules on the surface of metal. Therefore, the inhibition efficiency increases with an increase in the corrosion inhibitor concentration. The inhibition efficiencies obtained from EIS curves are in consistence with the results of potentiodynamic polarization at higher concentration $4.5 \times 10^{-4}$ M of suggested inhibitor (**2**), (see Tables 1, 2).

**Table 3.** Quantum calculation results of pyridinium salt derivative by using PM3 method

| |
|---|
| Inhibitor: pyridinium salt derivative |
| HOMO (eV): –12.4825 |
| LUMO (eV): –6.7773 |
| Energy gap ($\Delta E = E_{HOMO} - E_{LUMO}$) (eV): - 5.7052 |
| μ (Debye): 3.78 |
| Planarity: semi-planar |

The mechanism of corrosion inhibition could be explained by the formation of passive layers on the metal surface. The protective nature of the surface layers basis on different conditions: kind of electrolytes, PH of media, interaction nature between inhibitors and metal surface, incorporation of the inhibitor in the surface layer, chemical reactions, electrode potentials, concentration of the inhibitor, temperature, etc. [25]. The adsorption process of organic inhibitor could be controlled by competition interactions among the nature of the aggressive electrolyte, surface charge of the metal and the chemical structure of the organic inhibitor. In another words, adsorption energy of the interaction between inhibitor molecules and the metal surface is higher than that between electrolyte components and the metal surface. The adsorption mechanism of pyridinium salt derivative in 3.5% NaCl solution carried out by displacement of water molecules from the carbon steel surface and the sharing electrons between the hetero- atoms and metal surface. In addition, the positively charged inhibitor molecules encourage excess negative charges chloride ions to be vicinity for electrostatic interactions far from the metal surface. Thus we can conclude that inhibition of carbon steel corrosion in the presence of pyridinium salt derivative in 3.5% NaCl solution is due to the number of adsorption sites, their charge density and molecular size. All that could prepare the ability to form a kind of physisorption, chemisorption or a mixed adsorption mechanism with metal surface [26].

Finally, to study the relationship between molecular structure and inhibiting effect of the suggested inhibitor (**2**), molecular orbitals of semi-empirical calculations with PM3 method were used [27]. Semi-empirical calculations were achieved using the Hyperchem Program [28] with complete geometry optimization. Quantum calculations were performed for pyridinium salt derivative using more energetically stable conformations in the gas phase at 25°C (see Fig. 5). The calculated chemical parameters are given in Table 3 (energies of $E_{HOMO}$ and $E_{LUMO}$, energy gap ($\Delta E$) and other indices) are resulted of optimized molecular modeling system of suggested inhibitor by PM3 method. The PM3 method for estimation HOMO and LUMO isosurfaces for suggested inhibitor are shown in Fig. 6. It's clear from Fig. 6 that the repartition density of the HOMO and LUMO is preferentially localized on nitrogen (N) and oxygen (O) atoms and π- system of molecular modeling system of pyridinium salt derivate. Inhibition efficiency can be correlated to the energy levels of HOMO and LUMO and the difference between them and the smaller value of $\Delta E$ of an inhibitor makes its inhibition efficiency higher [29].

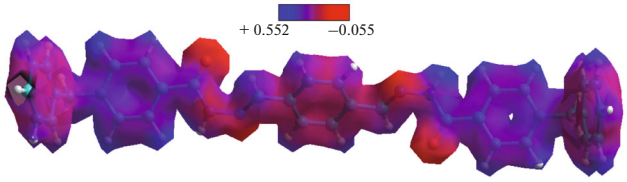


**Fig. 7.** Electrostatic potential maps for pyridinium salt derivative by using PM3 method.

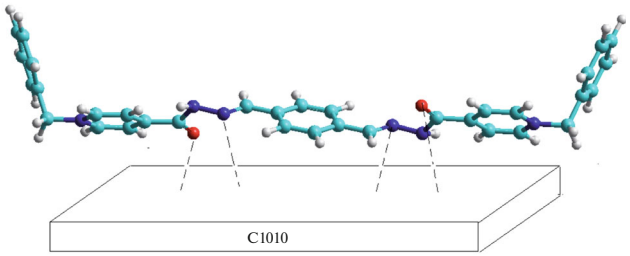


**Fig. 8.** Suggested physisorption of pyridinium salt derivative on C1010 carbon steel surface.

The inhibitor (**2**) has a high value of dipole moment due to existence of hetero atoms (N, O) and positively charge of the nitrogen atom of pyridine ring. This polarity of inhibitor molecule could be a good factor to improve the dipole-dipole interaction between organic molecule and metal steel surface and then to enhance corrosion inhibition [30].

Electrostatic potential maps for organic inhibitor model depicted in Fig. 7. This figure shows the non-uniform distribution of electron density and concentration of negative charges on the atoms N (C=N) and O (C=O) for organic inhibitor (**2**) model, which explains a high value of the calculated dipole moment (see Table 3).

Complete geometry optimization of pyridinium salt derivative as a molecular modeling system results semi-planarity configuration (see Table 3), which improved the inhibition efficiency by making the active sites (N (C=N) and O (C=O) atoms) closer to the surface of metal and that in turn improved the physisorption at high concentrations. Figure 8 shows suggested physisorption mechanism of pyridinium salt derivative on the surface of metal.

For this work, we can conclude that molecular modeling system is an appropriate tool to create correlation between theoretically calculated properties and experimentally determined inhibition efficiencies for corrosion process of pyridinium salt derivate in 3.5% NaCl solution at 25°C.

## 4. CONCLUSION

Pyridinium salt derivative was prepared and its structure was confirmed physically and also by spectroscopic techniques. Various concentrations of pyridinium salt derivative were used successfully as corrosion inhibitors for C1010 carbon steel in 3.5% NaCl solution at 25°C. The polarization parameters such as corrosion current density decreased significantly with increasing of the pyridinium salt concentration. The inhibition efficiencies obtained from EIS curves were in consistence with the results of potentiodynamic polarization at higher concentration of suggested inhibitor. A good correlation was found between theoretically calculated properties and experimentally determined inhibition efficiencies for corrosion process of pyridinium salt derivate in 3.5% NaCl solution by using molecular orbitals of semi-empirical calculations with PM3 method.

## ACKNOWLEDGMENT

The financial support of this work by the U.S. Department of State, with its implementing partner CRDF Global, under the Iraq Science Fellowship Program (ISFP) was gratefully acknowledged.

## REFERENCES

1. Sherif, E.M. and Park, S.M., *Electrochim. Acta,* 2006, vol. 51, p. 1313.
2. Ebenso, E.E., Obot, I.B., and Murulana, L.C., *Int. J. Electrochem. Sci.,* 2010, vol. 5, p. 1574.
3. Sanyal, B., *Prog. Org. Coat.,* 1981, vol. 9, p. 165.
4. Li, S., Chen, S., Lei, S., et al., *Corros. Sci.,* 1999, vol. 41, p. 1273.
5. Emregu, K.C. and Atakol, O., *Mater. Chem. Phys.,* 2003, vol. 82, p. 188.
6. Emregu, K.C. and Atakol, O., *Mater. Chem. Phys.,* 2004, vol. 83, p. 373.
7. Emregu, K.C., Kurtaran, R., and Atakol, O., *Corros. Sci.,* 2003, vol. 45, p. 2803.
8. Yurt, A., Ulutas, S., and Dal, H., *Appl. Surf. Sci.,* 2006, vol. 253, p. 919.
9. Kendig, M. and Jeanjaquet, S., *J. Electrochem. Soc.,* 2002, vol. 149, p. B47.
10. Ma, F., Li, W., Tian, H., Kong, Q., and Hou, B., *Int. J. Electrochem. Sci.,* 2012, vol. 7, p. 10909.
11. Popova, A., Christov, M., Vasilev, A., and Zwetanova, A., *Corros. Sci.,* 2011, vol. 53, p. 679.
12. Atia, A.A. and Saleh, M.M., *J. Appl. Electrochem.,* 2003, vol. 33, p. 171.
13. Achouri, M.El., Bensouda, Y., Gouttaya, H.M., et al., *Prog. Org. Coat.,* 2001, vol. 43, p. 267.
14. Mohite, P.B. and Bhaskar, V.H., *Orbital Elec. J. Chem. Campo Grande,* 2011, vol. 3, p. 117.
15. Daeniker, H.U. and Grob, C.A., *Org. Synth. Coll.,* 1973, vol. 5, p. 989.
16. Chauhan, L. and Gunasekaran, G., *Corros. Sci.,* 2007, vol. 49, p. 1143.
17. Hegazy, M.A., *Corros. Sci.,* 2009, vol. 51, p. 2610.

18. Jeyaprabha, C., Sathiyanarayanan, S., Muralidharan, S., and Venkatachari, G., *J. Braz. Chem. Soc.,* 2006, vol. 17, p. 61.
19. Growcock, F.B. and Jasinski, J.H., *J. Electrochem. Soc.,* 1989, vol. 136, p. 2310.
20. Ashassi-Sorkhabi, H., Seifzadeh, D., and Hosseini, M., *Corros. Sci.,* 2008, vol. 50, p. 3363.
21. Osman, M.M., Omar, A.M., and Al-Sabagh, A.M., *Mater. Chem. Phys.,* 1997, vol. 50, p. 271.
22. Goncalves, R.S., Azambuja, D.S., and Serpa Lucho, A.M., *Corros. Sci.,* 2002, vol. 44, p. 467.
23. Bommersbach, P., Alemany-Dumont, C., Millet, J., and Normand, B., *Electrochim. Acta,* 2005, vol. 51, p. 1076.
24. Raspini, I.A., *Werkst. Korros.,* 1985, vol. 36, p. 273.
25. Malik, M.A., Hashim, M.A., Shaeel, F.N., et al., *Int. J. Electrochem. Sci.,* 2011, vol. 6, p. 1927.
26. Noor, E.A. and Al-Moubaraki, A.H., *Mater. Chem. Phys.,* 2008, vol. 110, p. 145.
27. Shihab, M.S. and Al-Doori, H., *J. Mol. Struct.,* 2014, vol. 1076, p. 658.
28. *HyperChem 2002, Version 7.5,* Gainesville: Hypercube Inc., 2002.
29. Tang, Y., Yang, X., Yang, W., et al., *Corros. Sci.,* 2010, vol. 52, p. 1801.
30. Gao, G. and Liang, C., *Electrochim. Acta,* 2007, vol. 52, p. 4554.